Available online at www.sciencedirect.com
ScienceDirect
Trans. Nonferrous Met. Soc. China 33(2023) 1507−1521
Transactions of Nonferrous Metals Society of China
www.tnmsc.cn

Bioactive coating with antibacterial and anticorrosive properties deposited on ZA6-1 alloy bone implant

De-ren ZHAO[1,2], Dong CHEN[3], Xue FENG[4], Zi-lin CHEN[1,2], Chen JIN[1,2], Xiao-dong TAN[1,2], Yun-jie XIANG[1,2], Wen-bo JIAO[1,2], Ya-xing FANG[1,2], Li-qun XU[1,2], Yong-ping ZHANG[1,2], Xi RAO[1,2]

1. School of Materials and Energy, Southwest University, Chongqing 400715, China;
2. Chongqing Key Laboratory of Soft-matter Material Chemistry and Function Manufacturing, Southwest University, Chongqing 400715, China;
3. School of Food Science, Southwest University, Chongqing 400715, China;
4. Department of Clinical Laboratory, University-Town Hospital of Chongqing Medical University, Chongqing 401331, China

Received 9 November 2021; accepted 18 May 2022

Abstract: The commercial zinc aluminum alloy (ZA6-1) surface was functionalized with poly-(lactic-co-glycolic) acid (PLGA) containing sodium dodecyl sulfate (SDS) and levulinic acid (LA) for gaining antibacterial activity. A polymerized 3-aminopropyltriethoxysilane (APTES) layer was initially fabricated on the surface of ZA6-1 alloy to gain amino group, and the PLGA mixed with SDS/LA was subsequently immobilized on the as-treated surface through the electrostatic interaction between amino group and carboxyl group. The PLGA−SDS/LA coating on zinc alloy showed extremely good corrosion resistance with the degradation rate of 0.005 mm/a, which can be adjusted by varying the coating thickness. Furthermore, besides the good biocompatibility to osteoblasts, the PLGA−SDS/LA coating exhibited excellent antibacterial property, and the bactericidal rates against *Staphylococcus aureus* and *Escherichia coli* were 98.9% and 99.8%, respectively.

Key words: zinc alloy; polymer coating; antibacterial property; biocompatibility; corrosion behavior

1 Introduction

In order to eliminate the need for follow-up surgery to remove the implant when patients are completely recurred from diseases or accidents, materials scientists and doctors have recently paid significant attention to the application of biodegradable metals in biomedical area [1]. Zn and Zn-based alloys with moderate corrosion rates between Mg-based and Fe-based alloys, have demonstrated a promising potential for manufacturing biodegradable implants [2]. Zinc is a necessary trace element for human body, participating in basic life processes such as protein synthesis and energy metabolism [3]. Studies have shown that in the process of bone formation, zinc plays a two-way role in inhibiting bone resorption of osteoclasts and promoting osteogenesis of osteoblasts [4]. Zinc also promotes various processes of osteoblasts, including their proliferation, differentiation and collagen synthesis [5]. Thus, zinc and its alloys can provide potential biological applications as bone implants.

Compared with pure zinc, zinc alloys possessed significantly improved mechanical properties and biocompatibility [6]. Among those, zinc−aluminum alloys (ZA group) have displayed comprehensive

Corresponding author: Xi RAO, Tel: +86-23-68254092, E-mail: raoxiemail@swu.edu.cn;
Yong-ping ZHANG, Tel: +86-23-68254092, E-mail: zhangyyping@yahoo.com
DOI: 10.1016/S1003-6326(23)66199-0

physical and mechanical properties, including excellent casting properties, high strength and good plasticity [7]. Recently, WANG et al [8] reported zinc aluminum alloys ZA6-1 with better biocompatibility compared with pure zinc, implying the possible application of ZA6 in the biomedical area.

On the other hand, postoperative bacterial infection could bring huge health problems to mankind. Although the antibiotics have miraculous effects on bacterial infection, the abuse and overdose of traditional antibiotics could lead to the yield of drug-resistant bacteria [9]. Therefore, metal implants with no bacterial drug resistance, biological adaptation and broad spectrum anti-bacterial properties are a hotspot for clinical application. It was reported that the mixed solution of sodium dodecyl sulfate (SDS) and levulinic acid (LA) has good bactericidal effect [10,11]. However, such widely used chemicals in food industry were seldom used for biomedicine.

The direct bonding between SDS/LA and alloy metal substrate is an impractical challenge, as the solid chemical bond is difficult to be formed at the interface. Fortunately, 3-aminopropyltriethoxy-silane (APTES) has been confirmed to provide grafted functional groups for anchoring nano/micro particles [12−14]. Furthermore, polylactic acid glycolic acid (PLGA) loading SDS/LA can be coupled through the interaction between carboxyl groups and amino groups, and subsequently be immobilized on the surface [15], ensuring a long-term effective antibacterial activity.

In this study, a polymerized APTES layer was initially fabricated on the surface of ZA6-1 alloy, and the PLGA mixed with SDS/LA was subsequently immobilized on the as-treated surface to form a PLGA−SDS/LA coating. The morphology, chemical composition, corrosion performance, anti-bacterial properties and biocompatibility of the as-deposited coating were systematically studied and evaluated, aiming at building a novel biocompatible coating with excellent antibacterial activity for bone repair and tissue engineering applications.

2 Experimental

2.1 Material preparation

The surfaces of zinc alloy ZA6-1 (ZA6) foils (10 mm × 10 mm × 2 mm) were activated using plasma enhanced chemical vapor deposition (PECVD) method in argon plasma with power of 20 W for 1 min. The activated ZA6 was then immersed in ethanol solution containing 10% APTES for 30 min, and then was dried at 100 ℃ for 3 h. The APTES-treated samples were labeled as APTES functionalized ZA6. Afterwards, the solutions of PLGA and PLGA with 4 wt.% sodium dodecyl sulfate and 6 wt.% levulinic acid were spinning-coated on the APTES functionalized samples, respectively.

2.2 Characterization

Surface morphology was identified using scanning electron microscopy (SEM, JEOL, JSM−7800F). The surface roughness was observed using tapping mode atomic force microscope (AFM, Being Nano-Instrument Ltd., CSPM5500). The functional groups and elements were characterized and analyzed by Fourier transform infrared spectroscopy (FTIR, Perkin Elmer, Frontier) and Raman spectroscopy (Raman, HORIBA, Lab RAM HR Evolution). The chemical state and composition were measured by means of X-ray photoelectron spectroscopy (XPS, Thermo Fisher Scientific, ESCALAB 250Xi).

2.3 In vivo degradation behavior

The electrochemical tests, including electro-chemical impedance spectroscopy (EIS) and potentiodynamic polarization tests, were performed in an electrochemical station (AUTOLAB，model PGSTAT 302 N). The corrosion rate (v_{CR}) was calculated according to the following equation:

$$v_{CR}=3.27\times10^{-3}m_E J_{corr}/\rho=14.98\times10^{-3}\,J_{corr}.$$

where J_{corr} is corrosion current density (μA/cm^2), ρ is the density of corroding materials (g/cm^3), and m_E is the corresponding equivalent mass (g).

2.4 In vivo zinc ions release

The samples deposited with different coatings were immersed in the culture medium of Minimum Essential Media Alpha (MEM-α, Hyclone, USA) including 10 vol.% fetal bovine serum (FBS, NTC, Argentina) and 1 vol.% penicillin−streptomycin (Gibco, USA). For every 1 cm^2 of sample, 1.25 mL of culture medium was used and the samples were

soaked under 5 vol.% CO_2 humidified atmosphere at 37 ℃ for 3 d. Afterwards, the extracts were investigated using an inductively coupled plasma emission spectrometer (ICP, Optima 8000dv, ABI).

2.5 Antibacterial properties

The antibacterial properties of the samples were evaluated by a diffusion plate method [16]. 100 μL of bacterial suspension with a concentration of 1×10^6 CFU/mL was evenly distributed on agar dishes, and then the samples were placed in the middle and incubated in an incubator at 37 °C for 24 h. The antibacterial ability of the sample was evaluated by observing the size of the inhibition zone.

In addition, the method of co-culture of bacteria and samples [5] was used to evaluate the antibacterial ability. The samples were placed in a 24-well plate with the bacterial suspension with a concentration of 1×10^7 CFU/mL at 37 ℃ for 24 h. The adhesion of bacteria on the sample surface was observed by SEM, and the antibacterial rate was calculated by ImageJ software.

2.6 Hydrophilicity measurements

The static water contact angle (WCA) was measured using a contact angle goniometer (JC2000D, China) at a constant ambient temperature and humidity. A droplet (4 μL) of deionized water was put onto the sample surface to measure the WCA, and three measurements were performed on each surface of samples to obtain the average values along with the standard deviation for statistical accountability.

2.7 Cell viability

The MC3T3-E1 mouse pre-osteoblasts (MC3T3-E1 Subclone 14, Cell Bank of Chinese Academy of Sciences, China) were used to detect the cytotoxicity of coated and uncoated samples. For the indirect assays, cells were exposed to extract media from degraded samples according to ISO 10993—5 and ISO 10993—12. Briefly, Minimum Essential Media Alpha (MEM-α, Hyclone, USA) including 10 vol.% fetal bovine serum (FBS, NTC, Argentina) and 1 vol.% penicillin−streptomycin (Gibco, USA), was used as the culture medium for pre-osteoblasts. MTT assay was used to measure the cell viability.

2.8 Fluorescence staining and cell morphology

The cells were seeded in 24-well plates at a density of 1×10^4 cells/well, cultured for 24 h. Afterwards, the original medium was replaced with 50% diluted extract media and the cells were further cultured for 3 d [5]. The morphologies of the cells cultured in the extract medium were observed by confocal laser scanning microscope (CLSM, Zeiss 800).

2.9 Cell adhesion and morphology

Cells were seeded onto the coated and uncoated surfaces in a 6-well plate at a density of 1×10^5 cells/well and cultured at 37 °C for 3 d. The morphology of cells on the surface of the samples was observed by SEM.

2.10 Cell differentiation

The differentiation of pre-osteoblasts was measured by alkaline phosphatase activity kit [17]. The pre-osteoblasts were seeded in a 24-well plate at a density of 1×10^4 cells/well for 24 h with culture media, and then replaced the culture media with 50 vol.% diluted extract media for further culturing 3 and 7 d, respectively.

3 Results and discussion

3.1 Characterization of coatings

The surface morphology evolution and chemical composition of the films formed on the ZA6 surface were presented in Fig. 1. SEM micrograph shown in Fig. 1(a) indicated that before the coating deposition a rough surface with parallel scratches was seen on ZA6 samples. Figure 1(b) showed that the feature of the surface morphology hardly changed after the APTES functionalization. The high magnification image showed that plenty of white particles at nanoscale dispersed on the whole area of surface, indicating the existence of polymerized APTES layer. Figures 1(c) and (d) showed a clear and smooth surface after deposition. The change of both surface morphologies could correspond to the successful immobilization of PLGA or PLGA−SDS/LA using APTES as a grafting layer.

AFM was used to measure the roughness of APTES functionalized ZA6, PLGA deposited ZA6 and PLGA−SDS/LA deposited ZA6 coatings, respectively, as shown in Fig. 2. It could be seen

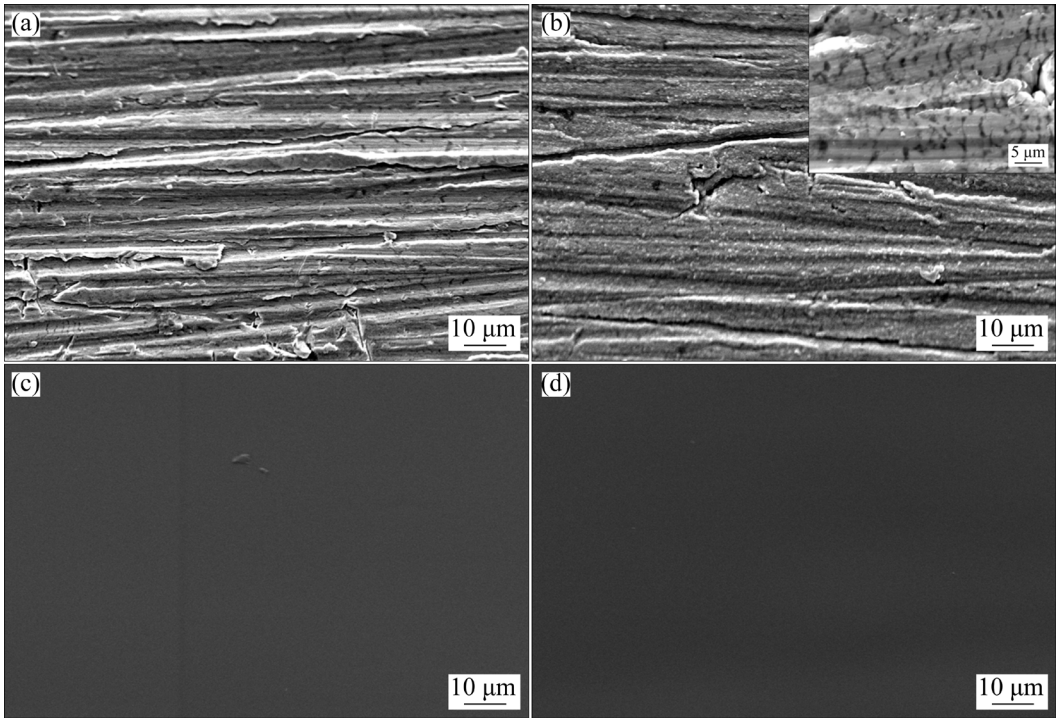

Fig. 1 SEM images of different surfaces: (a) Untreated ZA6; (b) APTES functionalized ZA6; (c) PLGA deposited ZA6; (d) PLGA−SDS/LA deposited ZA6

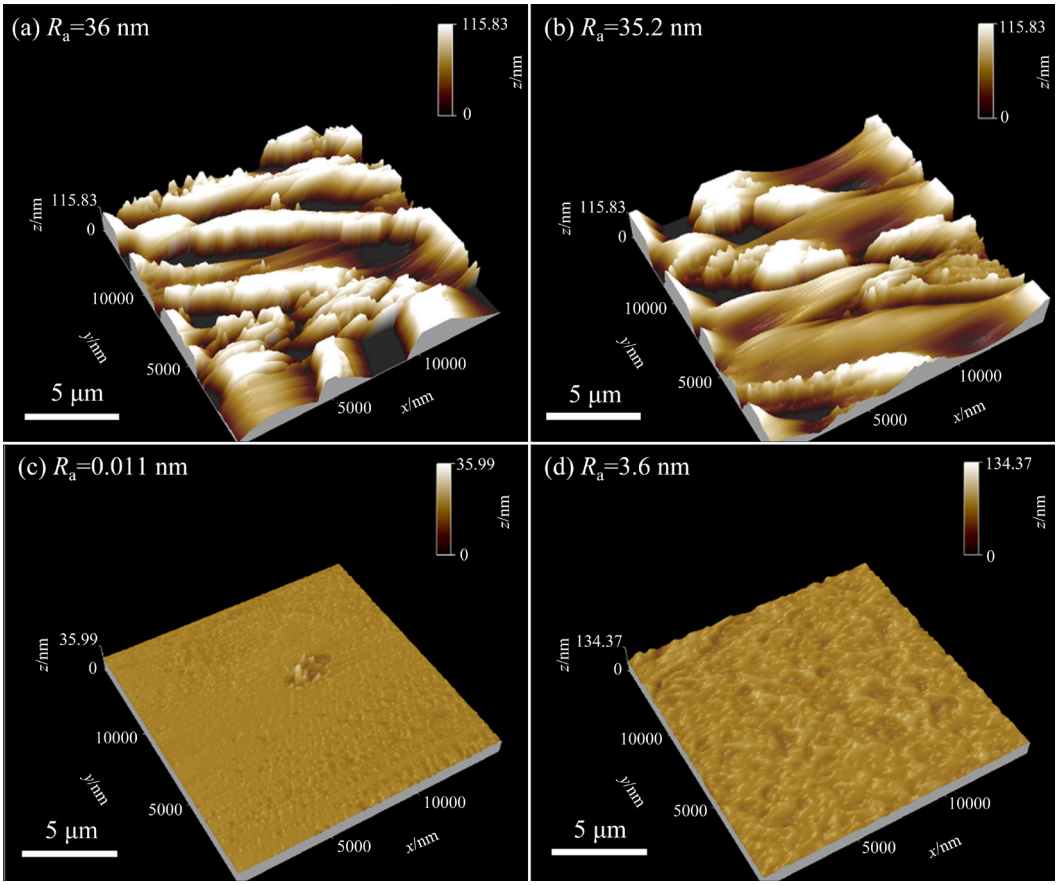

Fig. 2 AFM images of different surfaces: (a) Untreated ZA6; (b) APTES functionalized ZA6; (c) PLGA deposited ZA6; (d) PLGA−SDS/LA deposited ZA6

that the lowest roughness was obtained on the PLGA deposited surface. After the immobilization of SDS/LA, the roughness of surface was slightly decreased due to the corrosion of PLGA, which was consistent with the previous SEM results.

Furthermore, FTIR spectra recorded on the surface of ZA6 samples deposited with different coatings were shown in Figs. 3(a) and (b). Compared with the reference of untreated ZA6 samples, all the expected peaks of APTES were seen on the APTES functionalized surface as shown in Fig. 3(b): a strong absorption peak at about 914 cm^{-1} corresponding to Si—O—C and/or Si—O—Si [18], was probably due to the long chain of polymerized APTES molecules [19]; the absorption peak at 1630 cm^{-1} was related to N—H from amino groups [20], the peaks at 2851 and 2918 cm^{-1} corresponded to C—H from the alkyl groups [21], and the peak at 3358 cm^{-1} corresponded to N—H from amino groups. The spectrum of PLGA deposited surface presented in Fig. 3(a) showed different characteristics. The absorption band at 1243 cm^{-1} could be assigned to C—O of carboxylate groups of PLGA, the peaks at 2920 and 2999.7 cm^{-1} were contributed to $—CH_2$ groups, and the peak at 1748 cm^{-1} was assigned to C═O of ester group. As the SDS and LA showed almost the same absorption peaks as PLGA, the spectrum of SDS/LA immobilized coating showed similar characteristics in Fig. 3(a). It could only be speculated that the appearance of peak at 1082 cm^{-1} was due to the S—O of SDS.

Similar to the FTIR results, the Raman spectra of the APTES functionalized surface showed Raman peaks at 600.2, 1380, 2219 and 3392 cm^{-1}, corresponding to Si—O—Si, $—CH_3$, C—N and N—H, respectively (see Fig. 3(d)), indicating a successful functionalization of APTES on the surface [21]. The peak characteristics varied on the PLGA deposited surface: a peak at 2978.2 cm^{-1} corresponding to O—H vibration, a peak at 1791 cm^{-1} corresponding to ester group vibration, a peak at 1648 cm^{-1} corresponding to C═O, a peak at 1070 cm^{-1} corresponding to C—O—C, and a peak at 905 cm^{-1} corresponding to C—COO [22], which confirmed the existence of PLGA on the as-

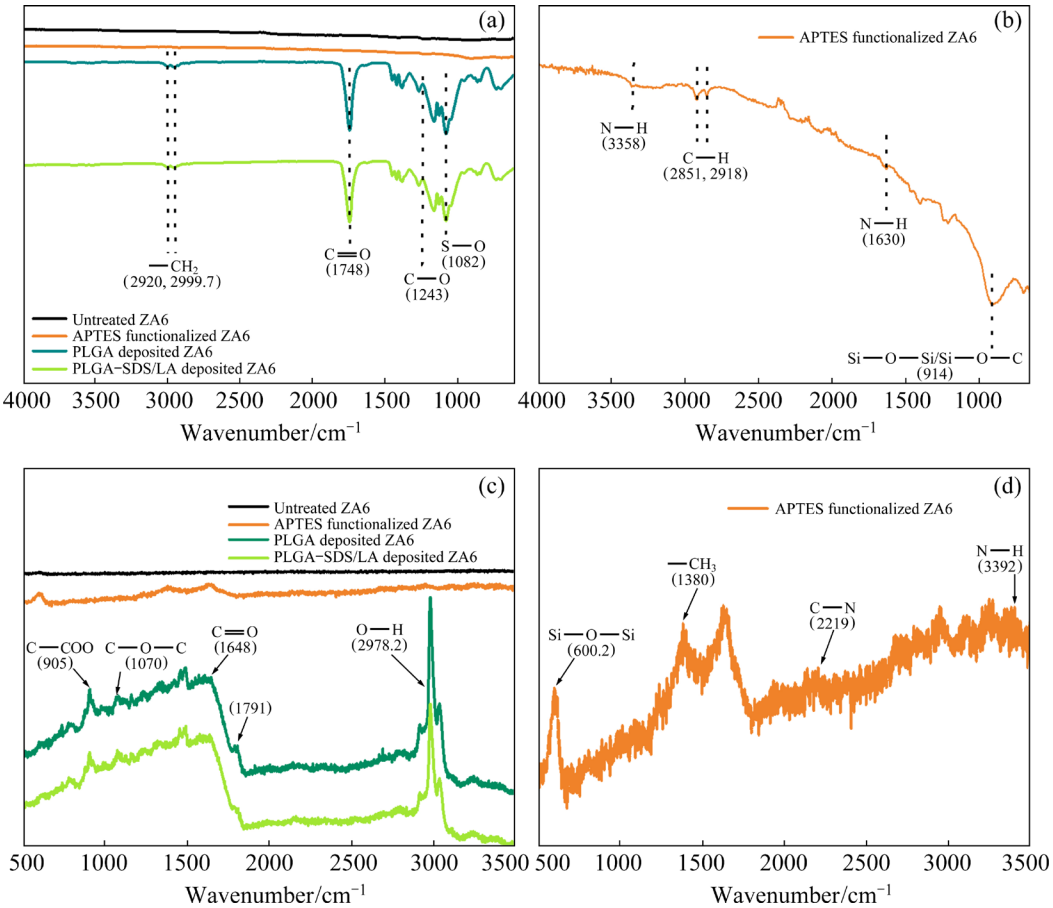

Fig. 3 FTIR spectra (a), high magnification FTIR spectrum (b), Raman spectra (c), and high magnification Raman spectrum (d)

functionalized surface (Fig. 3(c)). However, there is no obvious difference shown in the Raman spectra after SDS and LA were immobilized.

XPS was used for further investigation on the topmost surface composition. The survey scans and the high resolution spectra of C 1s, O 1s, N 1s, Si 2p, Na 1s and S 2p were shown in Fig. 4 and Table 1, respectively. As shown in Fig. 4(a), the survey spectra varied from each other, the presence of N 1s and Si 2p peaks could correspond to the existence of amino group and silyl group after APTES functionalization, while an additional Na 1s peak could contribute to the immobilization of SDS.

The deconvoluted C 1s peaks of APTES functionalized ZA6 centered at 285.0, 285.9, 287.1, 288.2 and 289.8 eV were attributed to C—C, C—N, C—O, C═O and C═O—O [23], respectively (Fig. 4(b)). The N 1s could be deconvoluted into two peaks: one at 400.7 eV corresponded to the amide functions of APTES; the other at 402.9 eV corresponded to the existence of $—NH_3^+$ [24], indicating the existence of protonated amino groups for grafting (Fig. 4(d)). Two deconvoluted peaks were observed in Si 2p: a peak at 102.5 eV corresponded to the Si—O—Zn group [22], confirmed the successful bonding of APTES on the surface of ZA6; a peak at 104.8 eV corresponded to Si—O—Si [12], indicating the polymerization of as-deposited APTES monomers (Fig. 4(d)). The O 1s could also be deconvoluted into two peaks: a peak at 532.3 eV corresponded to the O—Si group, agreeing with Si 2p, and a peak at 533.8 eV corresponded to O—C/O═C [20], agreeing with C 1s (Fig. 4(c)). Therefore, the binding energy values shown in XPS spectra for C 1s, Si 2p, N 1s and O 1s verified the existence of the APTES layer bound to ZA6 surface with protonated amino groups.

Figures 4(b) and (c) also displayed the high resolution C 1s and O 1s XPS spectra of PLGA deposited ZA6. Three peaks for C 1s were

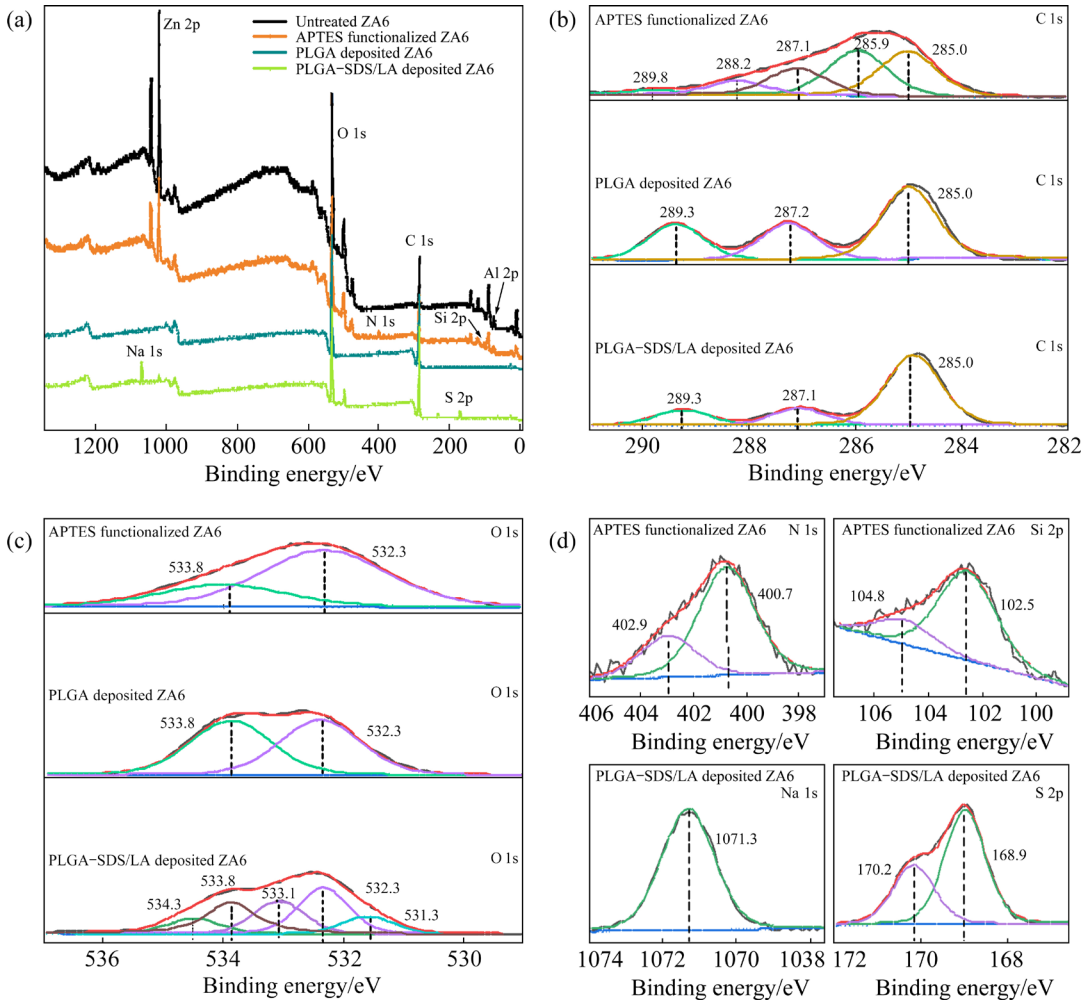

Fig. 4 XPS spectra: (a) Survey scan; (b) C 1s; (c) O 1s; (d) N 1s, Si 2p, Na 1s and S 2p

Table 1 Contents of element calculated from XPS (at.%)

Sample	Zn	Al	C	O	N	Si	S	Na
Untreated ZA6	9.93	10.91	39.1	40.06	−	−	−	−
APTES functional ZA6	4.99	10.86	40.32	37.48	3.81	2.54	−	−
PLGA deposited ZA6	−	−	66.48	31.75	1.77	−	−	−
PLGA-SDS/LA deposited ZA6	−	−	68.04	27.05	−	−	2.26	2.65

subsequently deconvoluted, as shown in Fig. 4(b): a peak at 285.0 eV is assigned to C—C, a peak at 287.2 eV to C—O, and a peak at 289.3 eV to C═O and C═O—O [25], which indicated the deposition of PLGA. Accordingly, the O 1s could be deconvoluted into two peaks at 532.3 and 533.8 eV, which were contributed to O—C/O═C [22]. It was also noticed that N 1s and Si 2p peaks were not observed on the surface of the PLGA deposited ZA6 (Fig. 4(a)). Concerning the detecting depth of XPS, such a result indicated that the thickness of as-deposited PLGA is much higher than 5 nm.

Furthermore, Figs. 4(b), (c) and (d) displayed the high resolution C 1s, O 1s, S 2p and Na 1s XPS spectra of PLGA−SDS/LA deposited ZA6. There were a peak at 287.1 eV relating to C—O, a peak at 285.0 eV relating to C—C and a peak at 289.3 eV relating to C═O and C═O—O [26] in C1s spectrum, agreeing with that of PLGA deposited ZA6. Differently, the O 1s peaks with binding energy values in the PLGA−SDS/LA deposited ZA6 surface at 531.3, 532.3, 533.1, 533.8 and 534.3 eV were attributed to —SO_3, O═C, O—H (coming from H_2O of air), O═S and O—C/O═C, respectively [27]. Furthermore, the Na 1s peak with binding energy values in the PLGA−SDS/LA deposited ZA6 surface at 1071.3 eV was attributed to Na^+. The S 2p could be deconvoluted into peaks at 168.9 and 170.2 eV, corresponding to the S—O and S═O groups, respectively [28]. Thus, all the results confirmed that the PLGA−SDS/LA coating was successfully deposited on the surface of ZA6.

3.2 Degradation behavior

The degradation behaviors of ZA6 samples deposited with different coatings were measured using a short-term polarization measurement including potentiodynamic polarization curves and Nyquist plots, presented in Fig. 5. The corrosion current density (J_{corr}) and corrosion potential (φ_{corr}) were evaluated by the Tafel extrapolation method, and the calculated electrochemical parameters were listed in Table 2.

APTES layer, PLGA coating and PLGA-SDS/LA coating showed different effects on the corrosion behavior of ZA6 alloy. Compared with untreated ZA6, the corrosion potential (φ_{corr}) of APTES functionalized ZA6, PLGA deposited ZA6 and PLGA-SDS/LA deposited ZA6 moved to a positive direction (Table 2), indicating that the polarization reactions of coated samples were delayed. Thus, the coatings could decrease the degradation rate of ZA6. However, the corrosion potential of PLGA−SDS/LA deposited ZA6 moved forward in the positive direction less than PLGA deposited ZA6, so the polarization reaction of PLGA−SDS/LA deposited ZA6 is faster than that of PLGA deposited ZA6. Accordingly, the polarization current density (J_{corr}) and corrosion rate (CR) of the three coated samples were lower than those of untreated ZA6. Although the polarization current density and corrosion rate of PLGA−SDS/LA deposited ZA6 were much lower than that of untreated ZA6 (0.33 μA/cm^2 vs 35.48 μA/cm^2; 0.005 mm/a vs 0.52 mm/a), they were still higher than those of PLGA deposited ZA6, which could be attributed to that the PLGA was corroded in advance by sodium dodecyl sulfate and levulinic acid during the immobilization [29]. It was noted that the corrosion rate could be attributed to the thickness of coating. An apparent thickness decrease occurred after SDS/LA immobilization, as shown in Figs. 6(a) and (b). Moreover, the compact PLGA coating structure could also be destroyed due to the existence of SDS/LA (Figs. 2(a) and (b)). Thus, the corrosion rate of ZA alloy could be feasibly adjusted by varying the loading amount of SDS/LA for changing coating thickness and morphology in this work.

The EIS Nyquist curves were shown in Figs. 5(b) and (c). There was only one capacitance ring in the impedance spectra of all the samples and the size was decreased as follows: PLGA−SDS/LA deposited ZA6≈PLGA deposited ZA6>APTES

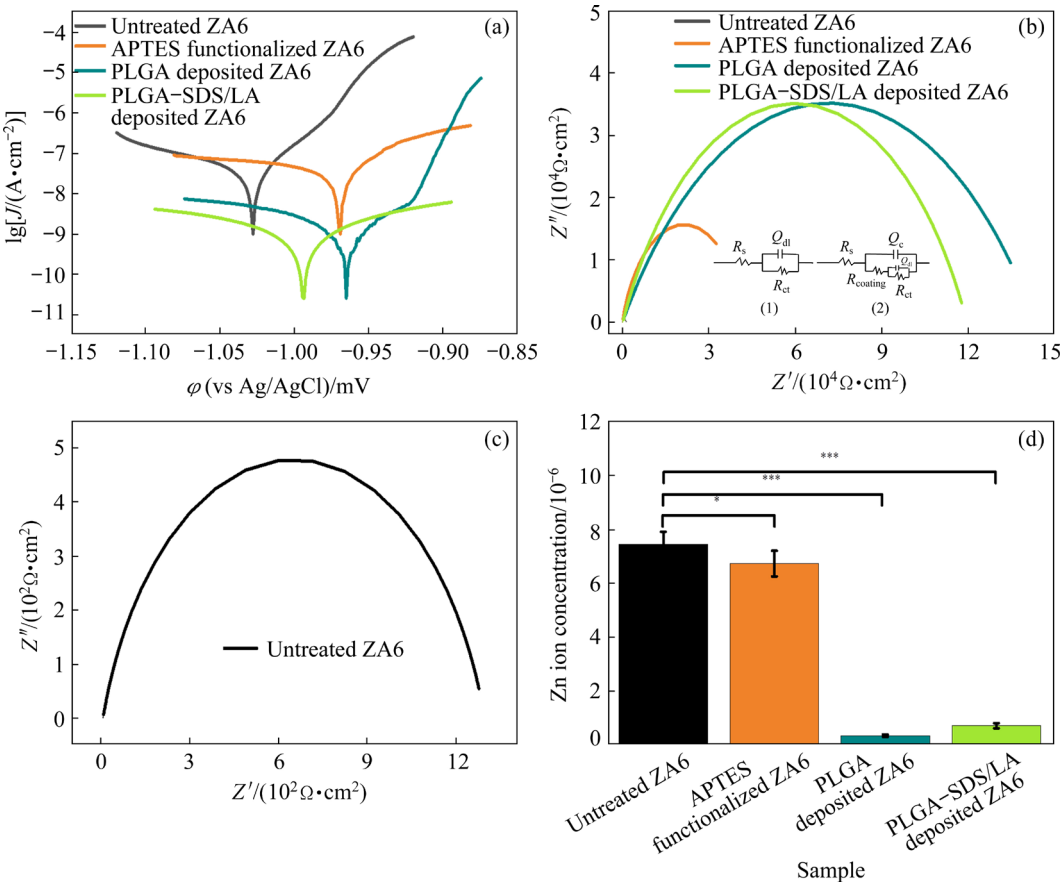

Fig. 5 Electrochemical corrosion behavior: (a) Potentiodynamic polarization curves; (b) Nyquist curves; (c) High magnification Nyquist curves; (d) Zn ion concentration of different samples (*p<0.05, **p<0.005, and ***p<0.0005)

Table 2 Electrochemical corrosion parameters of different samples in Hank's solution

Sample	φ_{corr} (vs Ag/AgCl)/mV	J_{corr}/(μA·cm^{-2})	Corrosion rate/(mm·a^{-1})
Untreated ZA6	−1020±1	35.48±1.7	0.52±0.007
APTES functionalized ZA6	−967±4	33.26±2.8	0.50±0.011
PLGA deposited ZA6	−950±3	0.20±0.01	0.003±0.0004
PLGA−SDS/LA deposited ZA6	−989±4	0.33±0.02	0.005±0.0001

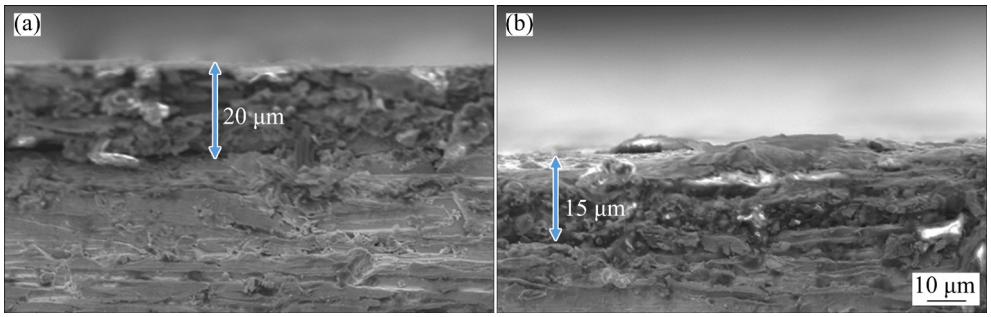

Fig. 6 Cross section of coating: (a) PLGA deposited ZA6; (b) PLGA−SDS/LA deposited ZA6

functionalized ZA6 >> untreated ZA6, according to the results of potentiodynamic polarization curves.

The equivalent circuit (EC) models corresponding to EIS were shown in the circuit diagrams (1) and (2) in Fig. 5(b). Diagram (1) corresponds to the equivalent circuit model of

untreated ZA6, R_s is the tested electrolyte resistance, R_{ct} is the charge transfer resistance of ZA6/electrolyte interface, and Q_{dl} is the double-layer capacitance of ZA6/electrolyte interface [29]. Differently, when the coatings deposit on the untreated ZA6 surface contact Hank's solution, electrochemical reaction will occur at the interface. As a consequence, the interface could be divided into two sub-interfaces, namely electrolyte/coating and ZA6/electrolyte interfaces. Therefore, the equivalent circuits of APTES functionalized ZA6, PLGA deposited ZA6 and PLGA−SDS/LA deposited ZA6 are composed of two resistors, as shown in diagram (2) in Fig. 5(b). The equivalent circuit consists of R_s (solution resistance) and constant phase element (Q), where Q_c represents coating capacitance and $R_{coating}$ represents coating resistance [26]; Q_{dl} is another component of Q, which represents the electric double-layer capacitance and charge transfer resistance R_{ct} in the vulnerable area [30]. For ZA6 substrate, Q and R_{ct} are related to hydroxide on ZA6 surface.

Compared with untreated ZA6 alloy, the corrosion active area of coating-deposited samples is significantly reduced, which could benefit in promoting corrosion resistance. On the other hand, a good corrosion resistance depends on the defect-free coating and the comprehensive physical barrier performance of the coating to electrolyte penetration into the coating and even to the substrate. Concerning the SEM image shown in Figs. 1(b), (c) and (d), more defects can be observed on the APTES deposited surface, while a dense and thick coating was covered on the PLGA or PLGA−SDS/LA deposited surface. Thus, a better corrosion resistance was obtained on PLGA and PLGA−SDS/LA deposited ZA6. Nevertheless, the existence of sodium dodecyl sulfate and levulinic acid could corrode the PLGA during the immersion, which probably leads to low corrosion resistance.

In terms of confirming the trend of corrosion resistance induced by coating deposition, the zinc ion concentrations in the extract for different samples immersed in Hank's solution for 3 d were then detected using ICP-MS and the results were shown in Fig. 5(d). The concentrations of released zinc ions for the PLGA deposited ZA6 and PLGA−SDS/LA deposited ZA6 groups were greatly reduced, compared with that for the untreated ZA6 group. According to the previous results of corrosion test, the concentration of zinc ions for the PLGA− SDS/LA deposited ZA6 groups was also slightly higher than that for the PLGA deposited ZA6 group, which was contributed to the corruption of PLGA by SDS/LA.

3.3 Antibacterial properties

The antibacterial activity of ZA6 samples deposited with different coatings to bacteria (*S. aureus*) was investigated and zone of inhibition was presented in Figs. 7(a)−(d) and Fig. 8(a). A significant zone of inhibition (ZOI) against *Staphylococcus aureus* was seen for the PLGA−SDS/LA deposited ZA6 group, and the radial diameter of ZOI was (13.3±0.3) mm.

Furthermore, the antibacterial activity of ZA6 samples deposited with different coatings was estimated using the co-culture of gram positive bacteria (*S. aureus*) and gram negative bacteria (*E. coli*) with samples. The morphologies of surface and antibacterial rates were shown in Figs. 7(e)−(l) and Figs. 8(b) and (c), respectively. As compared to the untreated ZA6 samples (12.74×10^5/mm^2), there was less *S. aureus* adhering and growing on the APTES functionalized ZA6 samples (10.40×10^5/mm^2) and the PLGA deposited ZA6 samples (3.78×10^5/mm^2). Especially, *S. aureus* barely appeared on the surface of PLGA−SDS/LA deposited ZA6 samples (0.14×10^5/mm^2) and the antibacterial rate of such samples was around 98.9% compared with that of untreated ZA6 samples. Accordingly, the surface of PLGA−SDS/LA deposited ZA6 samples showed the best antibacterial rate of 99.8% against *E. coli*, compared with the biofilm formed on the surface of the untreated ZA6 samples and the APTES functionalized ZA6 samples.

It should be noticed that zinc ions have a broad spectrum of antibacterial properties to inhibit the adhesion and growth of bacteria. As ZA6 alloy is biodegradable in the physiological environment, zinc ions could possibly diffuse from substrate to culture medium and exhibit high effect in killing gram positive bacteria and gram negative bacteria [31]. However, the ZA6 that showed the highest corrosion rate (Table 2) and the highest Zn^{2+} concentration released to the complete medium (Fig. 5(d)) did not exhibit bacterial activity, while the PLGA−SDS/LA deposited ZA6 that showed

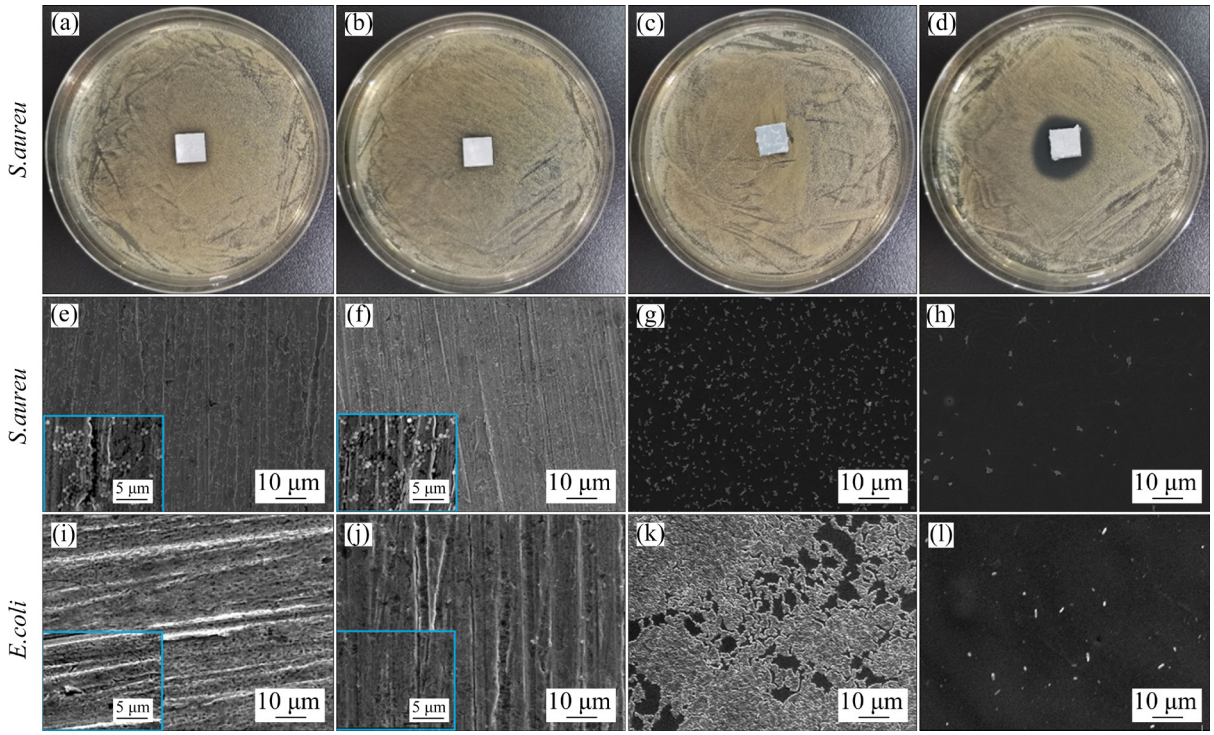

Fig. 7 Zone of inhibition and bacteria adhesion on surface: (a, e, i) Untreated ZA6; (b, f, j) APTES functionalized ZA6; (c, g, k) PLGA deposited ZA6; (d, h, l) PLGA−SDS/LA deposited ZA6

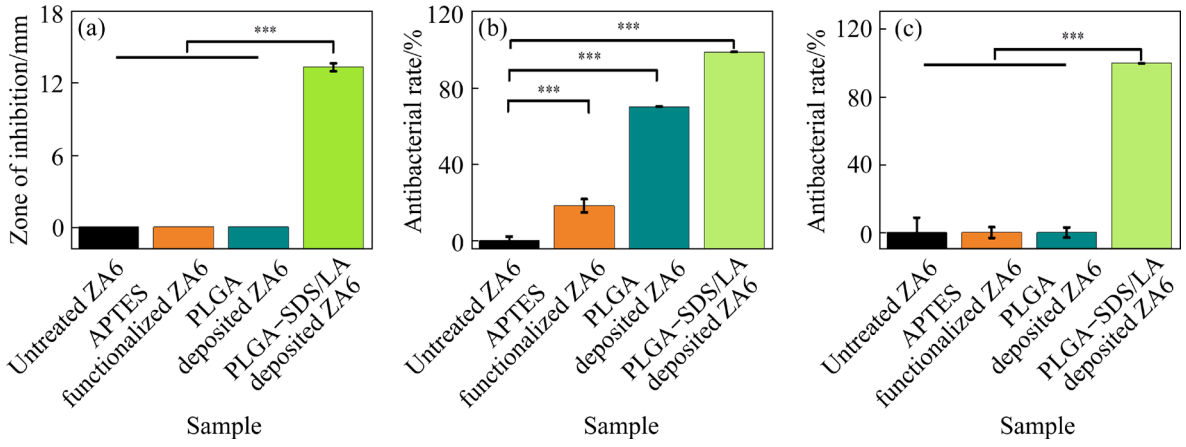

Fig. 8 Zone of inhibition of samples (a), and antibacterial rates for *S. aureus* (b) and *E. coli* (c) (*p<0.05, **p<0.005, and ***p<0.0005)

relatively low corrosion rate (Table 2) and the low Zn^{2+} concentration (Fig. 5(d)) exhibited excellent antibacterial performance, indicating that the release of zinc ions was not the essential reason for antibacterial activity in this work.

SDS is reported to destroy cell membranes as it can chelate divalent cations and denature proteins. With the decrease of the pH value, the antibacterial effect of SDS could be enhanced [32]. When SDS and LA are combined, LA can decrease the cytoplasmic pH of microorganisms through the ionization of undissociated acid molecules. On the other hand, LA affects the electrostatic charge of SDS molecules and cell surface, interferes with substrate transport, reduces proton power, chelates metal ions, and releases lipopolysaccharide from the outer membrane of bacteria [33]. Subsequently, more LA and SDS molecules are absorbed onto the bacteria cells due to the increase of cell permeability, leading to the damage of cytoplasmic membrane. Moreover, sodium dodecyl sulfate could be considered as an antiadhesive due to its

amphiphilicity, which means that the bacteria cells can hardly adhere on the SDS deposited surface [34]. Thus, SDS and LA complement each other and a synergistic effect on enhancing antibacterial performance can be obtained by combining SDS and LA.

3.4 Biomedical properties

As shown in Fig. 9(a), the WCA of the PLGA−SDS/LA deposited ZA6 samples was (12.8±2.1)°, indicating a significant hydrophilic surface. As a hydrophilic surface could facilitate more cell adhesion than hydrophobic surfaces, it should result in better cell adhesion and attachment.

The cell viability of MC3T3-E1 cells was displayed in Figs. 9(b)−(d). For 100% extracts, the relative cell viability of MC3T3-E1 osteoblasts cells after culturing for 1, 3 and 5 d was very low, for instance, (20.8±0.1)% and (29.4±0.5)% after culturing for 5 d for the untreated ZA6 and the PLGA−SDS/LA deposited ZA6 samples, respectively. The results indicated a larger cytotoxicity, in accordance with the previous studies that reported the presence of cytotoxic effects in original undiluted extracts of Zn-based alloys used in extract tests [2]. One possible explanation could be that the concentration of zinc ions in the extracts is much higher than the cellular tolerance of MC3T3-E1 for the Zn ion concentration [35]. It is well known that zinc ions are able to restrict the electron transport in the uncoupled mitochondrial [36], thus, a massive overdose of zinc ions could inhibit cell viability.

All the relative cell viabilities exhibited a trend of increase with continuous dilution of the sample extracts. The relative cell viability was higher than 80% and 100% when 50% and 25% extracts were cultured, respectively, implying no toxicity to MC3T3-E1 cells for ZA6 samples deposited with different coatings. Although, high doses of zinc ions

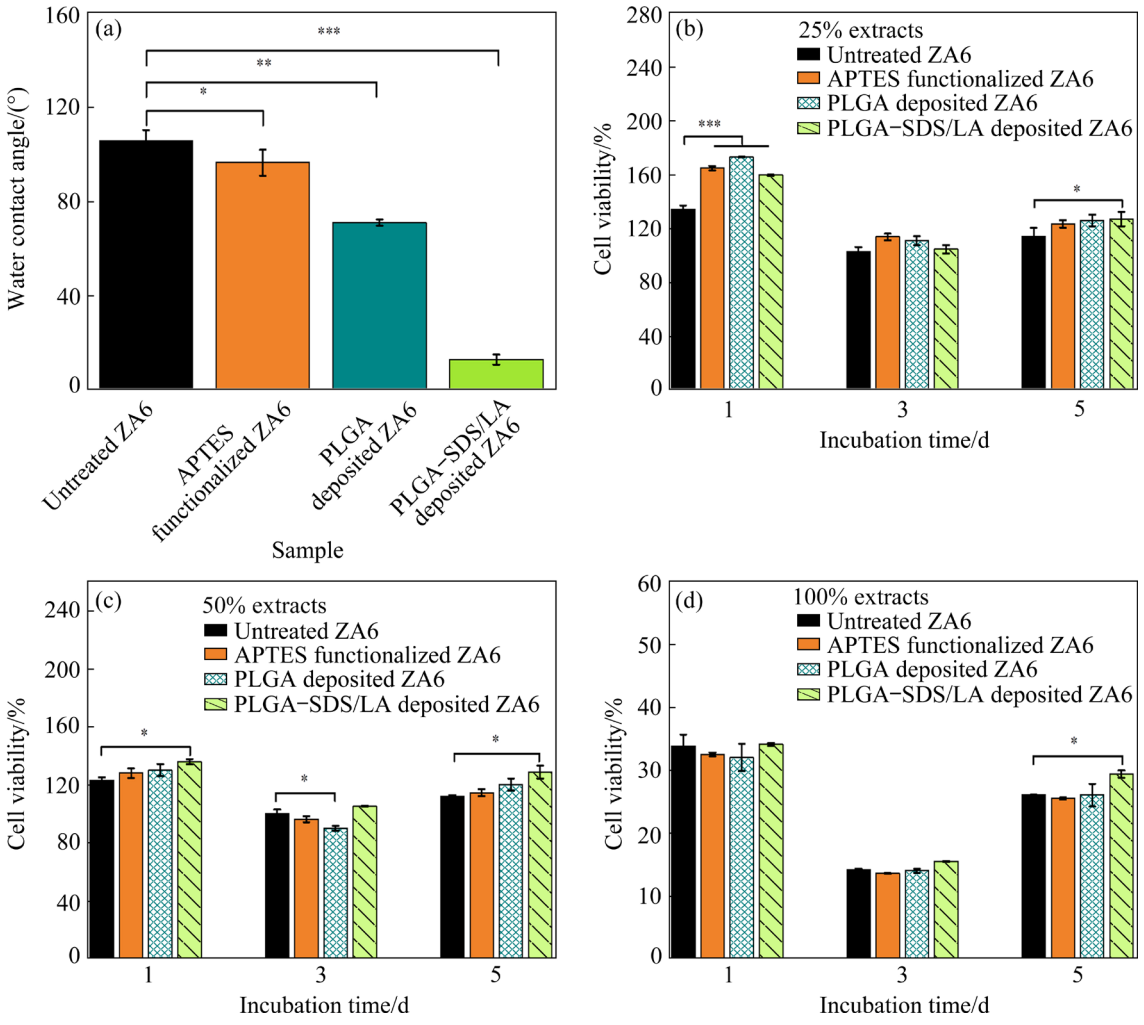

Fig. 9 Hydrophilicity property (a) and cell viability (b−d) (*p < 0.05, **p < 0.005, and ***p<0.0005)

were reported to show negative effort for cell viability, the low doses could result in the opposite consequence, as an appropriate amount of zinc ions could benefit cell viability, adhesion, proliferation, migration of osteoblast-like cells [37]. WANG et al [8] confirmed that the ZA6 alloy exhibited good biocompatibility with 50% extracts. Similarly, a good cell viability was observed in the untreated ZA6 group in this work when the extract was the same. Nevertheless, the PLGA− SDS/LA deposited ZA6 group showed the best cell viability of MC3T3-E1 cells cultured with 25% and 50% extracts for 5 d, indicating a better biocompatibility than that of ZA6 group.

As the Zn based alloys are biodegradable materials in physiological environment, it is suggested that a diluted extract must be applied for the biosafety evaluation in consideration of the distinct diversity between the in vitro and in vivo environment. FISCHER et al [38] suggested 10% extract to adjust the osmolality for cytotoxicity evaluation. WANG et al [8] used 20% and 50% extracts to carry out a good biocompatibility evaluation, respectively. In this work, both the 25% and 50% extracts were evaluated and demonstrated an excellent biocompatibility of the PLGA−SDS/LA deposited ZA6 samples.

Furthermore, the influence of ZA6 samples deposited with different coatings on the cell morphology was examined by means of cytoskeletal staining and the results were shown in Fig. 10. All the groups showed no significant difference for the number of viable cells. The morphology of MC3T3-E1 cells cultured with different extracts varied from each other. Several MC3T3-E1 cells displaying a round and unhealthy shape were observed for the untreated ZA6 group, while massive MC3T3-E1 cells displaying elongated shape with F-actin filaments were observed for the PLGA−SDS/LA deposited ZA6 group, suggesting that the PLGA−SDS/LA coating is favorable to the spreading of osteoblasts [39].

In vitro osteogenic differentiation activity was evaluated by quantitative analysis of alkaline phosphatase (ALP) activity, as shown in Fig. 11. All the groups of ZA6 samples deposited with different coatings showed good osteogenic differentiation activity. The ALP value was higher than 100% at 3 d and was close to 100% at 7 d, respectively. Especially, the PLGA−SDS/LA deposited ZA6 group exhibited the best ALP activity at 3 d, while all the groups showed a similar ALP activity at 7 d, indicating that PLGA−SDS/LA coating could benefit osteogenic differentiation.

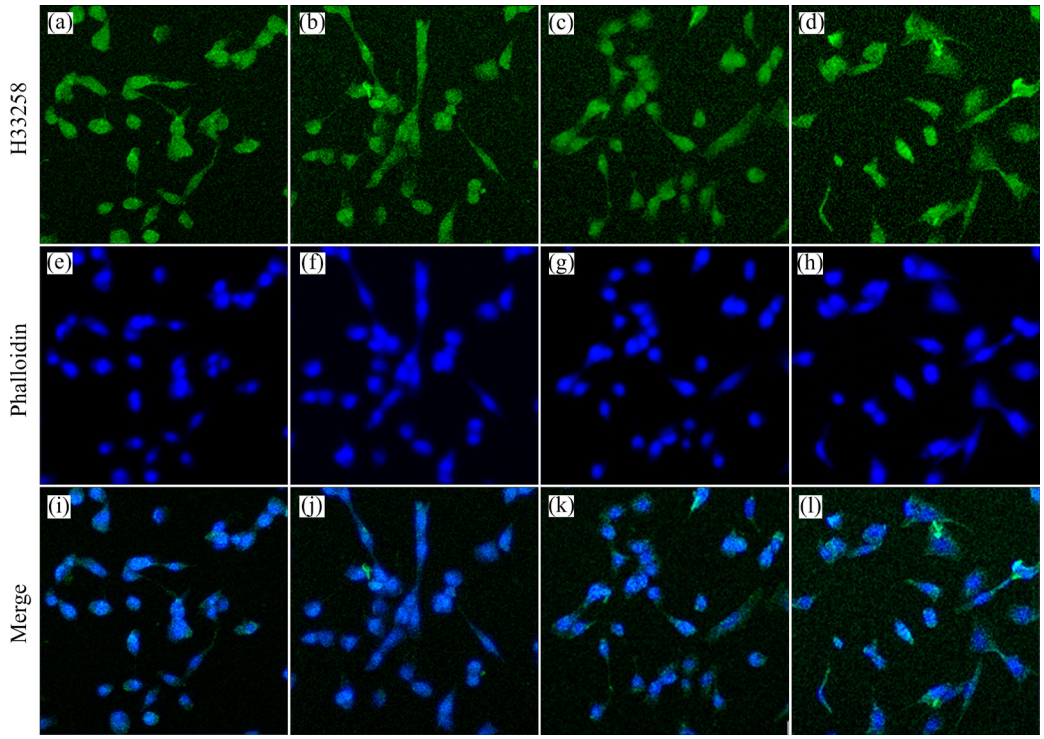

Fig. 10 Fluorescent images: (a, e, i) Untreated ZA6; (b, f, j) APTES functionalized ZA6; (c, g, k) PLGA deposited ZA6; (d, h, l) PLGA−SDS/LA deposited ZA6

The morphologies of MC3T3-E1 cells cultured on different surfaces were presented in Fig. 12. More adhered cells with a round shape were observed on the surface of untreated ZA6 samples and APTES functionalized ZA6 samples, indicating a less healthy state, while the cells displayed an elongated feature with several pseudopodia contacting the substrate after PLGA and PLGA−SDS/LA deposition. In general, a better cell adhesion often occurred on a rougher surface.

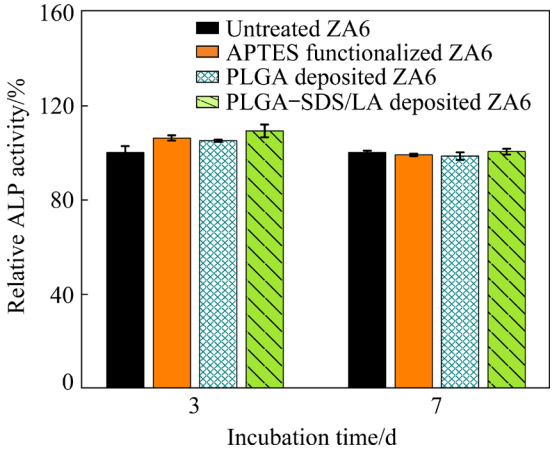

Fig. 11 Relative ALP activity of samples incubated for 3 and 7 d

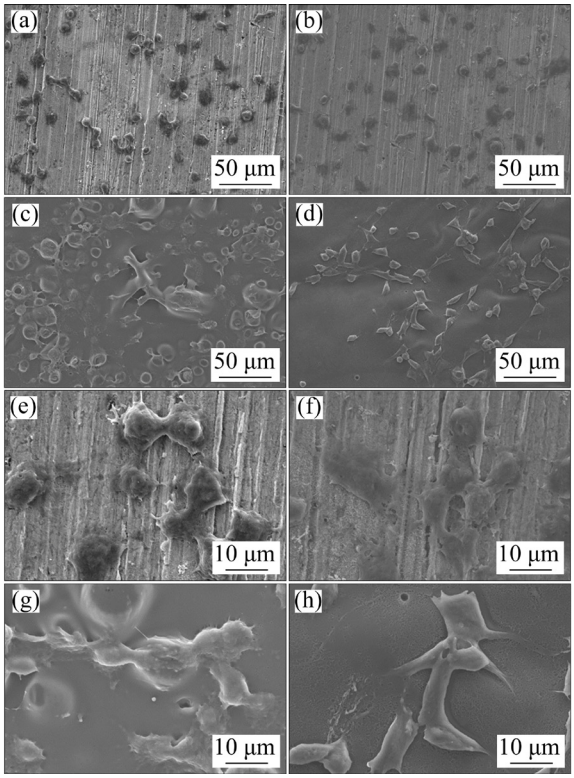

Fig. 12 Cell adhesion on surface: (a, e) Untreated ZA6; (b, f) APTES functionalized ZA6; (c, g) PLGA deposited ZA6; (d, h) PLGA−SDS/LA deposited ZA6

However, a reversed phenomenon was observed in this work, as the surface of the untreated ZA6 samples was rather rougher than that of the PLGA−SDS/LA deposited ZA6 samples. It could be possibly ascribed to the existence of SDS and LA and should be systematically investigated in the future work.

4 Conclusions

(1) A novel PLGA−SDS/LA coating was successfully fabricated on the commercial ZA6-1 alloy surface by functionalizing the substrate with APTES through the electrostatic interaction. The corrosion rate of substrate was decreased as the PLGA in coating improved the corrosion resistance, and it could be increased by loading SDS and LA due to the decrease of the thickness of PLGA layer during immobilization.

(2) The bactericidal rates of 98.9% against *S. aureus* and 99.8% against *E. coli* were achieved through a synergistic effect by combination of SDS and LA.

(3) The PLGA−SDS/LA coating exhibited good biocompatibility for adhering, proliferating and differentiating osteoblasts, confirming its promising potential for the surface modification for Zn-based orthopaedic implants.

Acknowledgments

The authors acknowledge supports from National Natural Science Foundation of China (No. 51801164), the Fundamental Research Funds for the Central Universities, China (No. XDJK2020C005), Chongqing Key Laboratory Fund of Soft-matter Material Chemistry and Function Manufacturing, China (No. 20200006), and Chongqing College Student Innovation and Entrepreneurship Program of Southwest University, China (No. 202010635076).

References

[1] KAFRI A, OVADIA S, YOSAFOVICH-DOITCH G, AGHION E. The effects of 4%Fe on the performance of pure zinc as biodegradable implant material [J]. Annals of Biomedical Engineering, 2019, 47: 1400−1408.

[2] SEYEDRAOUFI Z S, MIRDAMADI S. In vitro biodegradability and biocompatibility of porous Mg−Zn scaffolds coated with nano hydroxyapatite via pulse electrodeposition [J]. Transactions of Nonferrous Metals Society of China, 2015, 25: 4018−4027.

[3] LIU Bao-sheng, CAO Miao-miao, ZHANG Yue-zhong, HU Yong, GONG Chang-wei, HOU Li-feng, WEI Ying-hui. Microstructure, anticorrosion, biocompatibility and antibacterial activities of extruded Mg−Zn−Mn strengthened with Ca [J]. Transactions of Nonferrous Metals Society of China, 2021, 31: 358−370.

[4] CERQUEIRA A, ROMERO-GAVILÁN F, GARCÍA-ARNAEZ I, MARTINEZ-RAMOS C, OZTURAN S, ILORO I, AZKARGORTA M, ELORTZA F, IZQUIERDO R, GURRUCHAGA M, GOÑI I, SUAY J. Bioactive zinc-doped sol−gel coating modulates protein adsorption patterns and in vitro cell responses [J]. Materials Science and Engineering: C, 2021, 121: 111839.

[5] GUO Hui, XIA Dan-dan, ZHENG Yu-feng, ZHU Yuan, LIU Yun-song, ZHOU Yong-sheng. A pure zinc membrane with degradability and osteogenesis promotion for guided bone regeneration: In vitro and in vivo studies [J]. Acta Biomaterialia, 2020, 106: 396−409.

[6] GUO Hui, HE Ying, ZHENG Yu-feng, CUI Yong. In vitro studies of biodegradable Zn−0.1Li alloy for potential esophageal stent application [J]. Materials Letters, 2020, 275: 128190.

[7] ZHAO Li-chen, WANG Xin, WANG Tie-bao, XIA Yu-hang, CUI Chun-xiang. Mechanical properties and biodegradation of porous Zn−1Al alloy scaffolds [J]. Materials Letters, 2019, 247: 75−78.

[8] WANG C, YANG H T, LI X, ZHENG Y F. In vitro evaluation of the feasibility of commercial Zn alloys as biodegradable metals [J]. Journal of Materials Science & Technology, 2016, 32: 909−918.

[9] LIU Li, HUANG Bo, LIU Xiang-mei, YUAN Wei, ZHENG Yeng, LI Zhao-yang, YEUNG K W K, ZHU Sheng-li, LIANG Yan-qi, CUI Zhen-duo, WU Shui-lin. Photo-controlled degradation of PLGA/Ti_3C_2 hybrid coating on Mg−Sr alloy using near infrared light [J]. Bioactive Materials, 2021, 6: 568−578.

[10] ZHOU Man-li, DOYLE M P, CHEN Dong. Combination of levulinic acid and sodium dodecyl sulfate on inactivation of foodborne microorganisms: A review [J]. Critical Reviews in Food Science and Nutrition, 2020, 60: 2526−2531.

[11] LIU Chu-han, HUANG Yao-xin, CHEN Hai-qiang. Inactivation of *Escherichia coli* O157:H7 and *Salmonella enterica* on blueberries in water using ultraviolet light [J]. Journal of Food Science, 2015, 72: 391−396.

[12] LI Shuang-yang, HUANG Ping-sheng, YE Zhan-peng, WANG Ya-ping, WANG Wei-wei, KONG De-ling, ZHANG Jian-hua, DENG Lian-dong, DONG An-jie. Layer-by-layer zwitterionic modification of diverse substrates with durable anti-corrosion and anti-fouling properties [J]. Journal of Materials Chemistry B, 2019, 7: 6024−6034.

[13] RAO X, GUYON C, OGNIER S, DA SILVA B, CHU C L, TATOULIAN M, ABOU HASSAN A. High density gold nanoparticles immobilized on surface via plasma deposited APTES film for decomposing organic compounds in microchannels [J]. Applied Surface Science, 2018, 439: 272−281.

[14] CHEN Z L, ZHAO J J, JIN C, YUAN Y D, ZHANG Y P, TATOULIAN M, RAO X. Plasma deposited APTES: A potential film for biomedical application [J]. Materials Letters, 2020, 264: 127350.

[15] YU C C, CHEN Y W, YEH P Y, HSIAO Y S, LIN W T, KUO C W, CHUEH D Y, YOU Y W, SHYUE J J, CHANG Y C, CHEN P L. Random and aligned electrospun PLGA nanofibers embedded in microfluidic chips for cancer cell isolation and integration with air foam technology for cell release [J]. Journal of Nanobiotechnology, 2019, 17: 31.

[16] SHENG Y Y, YANG J J, ZHAO X Y, LIU H, CUI S G, CHEN L X, ZENG R, WANG X J, HUANG C H, LI W. Development and in vitro biodegradation of biomimetic zwitterionic phosphorylcholine chitosan coating on Zn_1Mg alloy [J]. ACS Applied Materials & Interfaces, 2020, 12: 54445−54458.

[17] SHEIKH F A, JU H W, MOON B M, LEE O J, KIM J H, PARK H J, KIM D W, KIM D K, JANG J E, KHANG G, PARK C H. Hybrid scaffolds based on PLGA and silk for bone tissue engineering [J]. Journal of Tissue Engineering and Regenerative Medicine, 2016, 10: 209−221.

[18] ZHOU L, FAN L, ZHANG F M, JIANG Y H, CAI M, DAI C, LUO Y A, TU L J, ZHOU Z N, LI X J, NING C Y, ZHENG K, BOCCACCINI A R, TAN G X. Hybrid gelatin/oxidized chondroitin sulfate hydrogels incorporating bioactive glass nanoparticles with enhanced mechanical properties, mineralization, and osteogenic differentiation [J]. Bioactive Materials, 2021, 6: 890−904.

[19] KIM J Y, SEIDLER P, WAN L S, FILL C. Formation, structure, and reactivity of amino-terminated organic films on silicon substrates [J]. Journal of Colloid and Interface Science, 2009, 329: 114−119.

[20] NAYAK N, HUERTAS R, CRESPO J G, PORTUGAL C A M. Surface modification of alumina monolithic columns with 3-aminopropyltetraethoxysilane (APTES) for protein attachment [J]. Separation and Purification Technology, 2019, 229: 115674.

[21] FOTSING P N, BOUAZIZI N, WOUMFO E D, MOFADDEL N, LE DERF F, VIEILLARD J. Investigation of chromate and nitrate removal by adsorption at the surface of an amine-modified cocoa shell adsorbent [J]. Journal of Environmental Chemical Engineering, 2021, 9: 104618.

[22] LIU J, XI T F. Enhanced anti-corrosion ability and biocompatibility of PLGA coatings on MgZnYNd alloy by BTSE−APTES pre-treatment for cardiovascular stent [J]. Journal of Materials Science & Technology, 2016, 32: 845−857.

[23] ACRES R G, ELLIS A V, ALVINO J, LENAHAN C E, KHODAKOV D A, METHA G F, ANDERSSON G G. Molecular structure of 3-aminopropyltriethoxysilane layers formed on silanol-terminated silicon surfaces [J]. The Journal of Physical Chemistry C, 2012, 116: 6289−6297.

[24] RAO X, TATOULIAN M, GUYON C, OGNIER S, CHU C L, ABOU HASSAN A. A comparison study of functional groups (amine vs. thiol) for immobilizing AuNPs on zeolite surface [J]. Nanomaterials, 2019, 9: 1034.

[25] ZHENG Y F, LI C, LI C J, CAI W, ZHAO L C. Surface characteristics and biological properties of paclitaxel-embedding PLGA coatings on TiNi alloy [J]. Materials Science and Engineering: A, 2006, 438: 1119−1123.

[26] RIKHARI B, MANI S P, RAJENDRAN N. Electrochemical behavior of polypyrrole/chitosan composite coating on Ti metal for biomedical applications [J]. Carbohydrate Polymers, 2018, 189: 126−137.

[27] GENG X, LV L, ZHANG T, TANG S W. The regulating mechanism of $MgCO_3·3H_2O$ whisker growth orientation

with the presence of SDS [J]. Journal of CO_2 Utilization, 2020, 42: 101307.
[28] ORTIZ G R, LARTUNDO-ROJAS L, SAMANIEGO-BENITEZ J E, JIMENEZ-FLORES Y, CALDERON H A, MANTILLA A. Photocatalytic behavior for the phenol degradation of ZnAl layered double hydroxide functionalized with SDS [J]. Journal of Environmental Management, 2021, 277: 111399.
[29] ASADI N, NADERI R, MAHDAVIAN M. Doping of zinc cations in chemically modified halloysite nanotubes to improve protection function of an epoxy ester coating [J]. Corrosion Science, 2019, 151: 69−80.
[30] BAKHSHESHI-RAD H R, HAMZAH E, ISMAIL A F, AZIZ M, KARAMIAN E, IQBAL N. Bioactivity, in-vitro corrosion behavior, and antibacterial activity of silver−zeolites doped hydroxyapatite coating on magnesium alloy [J]. Transactions of Nonferrous Metals Society of China, 2018, 28: 1553−1562.
[31] QU X H, YANG H T, JIA B, WANG M Q, YUE B, ZHENG Y F, DAI K R. Zinc alloy-based bone internal fixation screw with antibacterial and anti-osteolytic properties [J]. Bioactive Materials, 2021, 6: 4607−4624.
[32] CANNON J L, AYDIN A, MANN A N, BOLTON S L, ZHAO T, DOYLE M P. Efficacy of a levulinic acid plus sodium dodecyl sulfate-based sanitizer on inactivation of human norovirus surrogates [J]. Journal of Food Protection, 2012, 75: 1532−1535.
[33] RIGOTTI R T, CORREA J A F, MAIA N J L, CESARO G, ROSA E A R, de MACEDO R E F, LUCIANO F B. Combination of natural antimicrobials and sodium dodecyl sulfate for disruption of biofilms formed by contaminant bacteria isolated from sugarcane mills [J]. Innovative Food Science & Emerging Technologies, 2017, 41: 26−33.
[34] RAYBAUDI-MASSILIA R M, MOSQUEDA-MELGAR J, SOBRINO-LOPEZ A, SOLIVA-FORTUNY R, MARTIN-BELLOSO O. Use of malic acid and other quality stabilizing compounds to assure the safety of fresh-cut “FUJI” apples by inactivation of *Listeria monocytogenes*, *Salmonella enteritidis* and *Escherichierichia coli* O157:H7 [J]. Journal of Food Safety, 2009, 29: 236−252.
[35] LU Tao, LI Jian, QIAN Shi, CAO Hui-liang, NING Cong-qin, LIU Xuan-yong. Enhanced osteogenic and selective antibacterial activities on micro-/nano-structured carbon fiber reinforced polyetheretherketone [J]. Journal of Materials Chemistry B, 2016, 4: 2944−2953.
[36] SENSI S L, TON-THAT D, SULLIVAN P G, JONAS E A, GEE K R, KACZMAREK L K, WEISS J H. Modulation of mitochondrial function by endogenous Zn^{2+} pools [J]. Proceedings of the National Academy of Sciences of the United States of America, 2003, 100: 6157−6162.
[37] WANG Yan-hong, LI Ke-jin, MAO Li, HU Xin, ZHAO Wen-jie, HU An, LIAN Hong-zhen, ZHENG Wei-juan. Effects of exogenous zinc on cell cycle, apoptosis and viability of MDAMB231, HepG2 and 293 T cells [J]. Biological Trace Element Research, 2013, 154: 418−426.
[38] FISCHER J, PROEFROCK D, HORT N, WILLUMEIT R, FEYERABEND F. Improved cytotoxicity testing of magnesium materials [J]. Materials Science and Engineering: B, 2011, 176: 830−834.
[39] GUO Yun-ting, JIA Si-qi, QIAO Lu, SU Ying-chao, GU Rui, LI Guang-yu, LIAN Jian-she. A multifunctional polypyrrole/zinc oxide composite coating on biodegradable magnesium alloys for orthopedic implants [J]. Colloids and Surfaces B: Biointerfaces, 2020, 194: 111186.

ZA6-1 锌合金骨植入体表面沉积抗菌及耐腐蚀型生物活性涂层

赵德人[1,2]，陈 栋[3]，封 雪[4]，陈滋霖[1,2]，金 宸[1,2]，谭小东[1,2]，
向芸颉[1,2]，焦文博[1,2]，方亚星[1,2]，徐立群[1,2]，张永平[1,2]，饶 席[1,2]

1. 西南大学 材料与能源学院，重庆 400715；
2. 西南大学 软物质材料化学与功能制造重庆市重点实验室，重庆 400715；
3. 西南大学 食品科学学院，重庆 400715；
4. 重庆医科大学 附属大学城医院 检验科，重庆 401331

摘 要：通过在商用 ZA6-1 锌合金表面沉积负载十二烷基硫酸钠(SDS)和乙酰丙酸(LA)的聚乳酸羟基乙酸共聚物(PLGA)赋予其抗菌性能。首先，在 ZA6-1 锌合金表面聚合化沉积 APTES 接枝层，获得氨基官能团；随后，利用氨基官能团与羧基官能团的正负电荷吸引作用使与 SDS/LA 混合的 PLGA 负载于基体表面。所制备的 PLGA−SDS/LA 涂层具有良好的耐腐蚀能力，其腐蚀速率低至 0.005 mm/a，并且可通过改变涂层厚度对其进行调控。该涂层除具有良好的成骨细胞相容性外，还具有优良的抗菌性能，其对金黄色葡萄球菌和大肠杆菌的抗菌率分别达到 98.9%和 99.8%。

关键词：锌合金；聚合物涂层；抗菌性能；生物相容性；腐蚀行为

(Edited by Wei-ping CHEN)